Analyst

Accepted Manuscript

This is an *Accepted Manuscript*, which has been through the Royal Society of Chemistry peer review process and has been accepted for publication.

Accepted Manuscripts are published online shortly after acceptance, before technical editing, formatting and proof reading. Using this free service, authors can make their results available to the community, in citable form, before we publish the edited article. We will replace this *Accepted Manuscript* with the edited and formatted *Advance Article* as soon as it is available.

You can find more information about *Accepted Manuscripts* in the Information for Authors.

Please note that technical editing may introduce minor changes to the text and/or graphics, which may alter content. The journal's standard Terms & Conditions and the Ethical guidelines still apply. In no event shall the Royal Society of Chemistry be held responsible for any errors or omissions in this *Accepted Manuscript* or any consequences arising from the use of any information it contains.

ROYAL SOCIETY OF CHEMISTRY

www.rsc.org/analyst

Towards deep-UV surface-enhanced resonance Raman spectroscopy of explosives: Ultrasensitive, real-time and reproducible detection of TNT

Shankar K. Jha,[†] *Yasin Ekinci,* [*†‡] *Mario Agio,*[§] *Jörg F. Löffler*[†]

[†]Laboratory of Metal Physics and Technology, Department of Materials, ETH Zürich, Switzerland

[‡]Laboratory of Micro- and Nanotechnology, Paul Scherrer Institute, 5232 Villigen-PSI, Switzerland

[§] National Institute of Optics (INO-CNR) and European Laboratory for Nonlinear Spectroscopy (LENS), via Nello Carrara 1, 50019 Sesto Fiorentino (FI), Italy

Corresponding author: yasin.ekinci@psi.ch

KEYWORDS: UV, Deep-UV, resonance Raman, SERS, SERRS, 2,4,6-trinitrotolouene, TNT, detection, explosive, aluminum, nanoparticle, plasmonics.

Abstract

We report ultrasensitive and label-free detection of 2,4,6-trinitrotolouene (TNT) deposited by drop coating using deep-ultraviolet surface-enhanced resonance Raman scattering (DUV-SERRS). Well-defined aluminum nanoparticle arrays as SERRS substrate and 257 nm excitation wavelength enabled highly reproducible and real-time detection of TNT down to the detection limit of attogram level in quantity. This extreme sensitivity can be further improved by optimization of the nanostructured substrates. DUV-SERRS promises a large impact on public safety and security, as it can be readily extended to other explosives and hazardous materials.

Analyst Accepted Manuscript

Rapid and reliable detection of trace quantities of explosive and hazardous materials is critical for public safety, homeland security, and environmental protection. Many detection techniques that rely on different physical and chemical mechanisms have been explored and developed in the past decades [1-3]. Today's world of ever-increasing rate of transport of goods and public travel as well as the recent increase in the use of explosives in terrorist activities against civilians urges the improvement of the established methods or the development of novel techniques that exhibit better performances in terms of sensitivity, speed of analysis, reliability, portability, and costs.

2, 4, 6-trinitrotoluene (TNT), a military grade explosive, is widely used in landmines and other ordnance devices. Apart from being a highly potent explosive, it presents a widespread ecological threat causing extensive toxic contamination of soil and water due to its phytotoxicity even at concentration levels of parts-per-million (ppm) [4,5]. Most widely used methods of TNT detection outside the lab include olfaction, i.e. sniffer dogs, and ion mobility spectrometry (IMS) detectors [1-3]. The popularity of IMS detectors is based on their speed (typically less than a 0.1 s) and their ease of use. However, their quantitative detection limit is on the order of 10-100 picograms and it shows significant variation depending on the device. Spectroscopic methods are one of the several ways currently being explored for detection of trace quantities of explosives. Among them, fluorescence based detection, which makes use of the fact that electron deficient explosive molecules cause extensive quenching of the emission from fluorescing polymers, yields detection limit of attograms of TNT which however is limited in specificity [6].

Raman scattering, a vibrational spectrometric technique, is a promising approach for trace detection of explosives as it provides molecular specificity based on the "vibrational fingerprint" of the molecules. Moreover, its non-destructive nature and the fact that it requires little or no sample preparation makes it an ideal technique for usage in field settings and hostile environments [2,3,7]. Several groups have also explored standoff detection of explosives using Raman spectroscopy [8,9]. However, the technique suffers from low sensitivity, with a detection limit of the order of nanograms of TNT [2,7] due to the inherently weak Raman scattering cross-sections of molecules. In addition, background fluorescence reduces the signal-to-noise ratio (SNR) [3,7].

Analyst Accepted Manuscript

Surface-enhanced Raman scattering (SERS) is a widely used technique for improving the Raman signal. The electromagnetic (EM) field enhancement that occurs near metal nanostructures due to the excitation of localized surface plasmon resonances (LSPRs) is considered to be the dominant signal enhancement mechanism [10-12]. There are several reports that explore SERS as a technique for sensitive detection of explosive materials [13-20], with limits in the range of 1-200 picograms in most cases. Using a colloidal solution as SERS-active medium detection of TNT as low as femtograms has been demonstrated [17].

The general choice of the excitation wavelength in Raman scattering has been in the NIR to minimize sample fluorescence, which severely affects the SNR [7, 13]. However, the use of longer excitation wavelengths reduces the Raman cross section owing to its fourth power dependence on the excitation frequency. Hence, the use of DUV wavelengths can be an effective strategy to significantly improve both the Raman signal and the SNR by respectively increasing the cross section and separating the Raman peaks from the fluorescence background [9, 21].

Resonance Raman (RR) scattering, which occurs when the incident frequency matches the electronic transition energy, results in an increased Raman cross section and hence is an alternative method of improving the Raman signal. TNT has a broad electronic absorption band with an absorption maximum around 230 nm [22, 23]. The use of DUV excitation enables the RR effect and has been employed successfully to increase the detection sensitivity of TNT [8, 9, 22-24]. It is thus clear that the combination of RR and SERS in the DUV, i.e. DUV-SERRS offers a powerful approach in the quest of a fast and label-free detection with ultimate sensitivity and specificity. Indeed, there is an increasing interest in this novel technique and its application to various analytes of interest has been demonstrated [26-28].

In this Letter we explore the sensitivity of DUV-SERRS for TNT detection using Al NP arrays as substrates. Al is emerging as a material of choice for plasmonic applications in the UV and DUV as Al nanostructures offer good surface stability and strong LSPRs with reproducible surface enhancements in this wavelength range [29-34]. We demonstrate that DUV-SERRS has a great potential for ultrasensitive, reproducible and fast detection of explosive materials and thereby can have a great impact on public security.

For our studies Al NP arrays were fabricated on fused silica substrates (further details can be found in Supporting Information) using extreme-UV interference lithography (EUV-IL). This

Analyst Accepted Manuscript

method enables fabrication of periodic nanostructures over large areas with high resolution and high throughput on nonconductive surfaces [35]. For absorption, LSPR, and Raman scattering measurements a home-made UV microscope was used (see Supporting Information.), which is coupled to a spectrometer with a UV optimized, back illuminated, liquid nitrogen cooled CCD detector. The micro-Raman spectra were acquired in 180° backscattering configuration using 257-nm-wavelength continuous wave (CW) laser excitation from an Ar ion laser. The laser spot size at the sample using an objective of 0.4 NA was measured to be ~1 μm.

TNT as 1 mg/ml solution in acetonitrile (ACN) (Cerilliant Corporation) was further diluted using HPLC grade ACN (Sigma-Aldrich). TNT molecules were deposited onto the substrates by the drop-coating method. Drop coating is one of the easiest ways of analyte deposition and it is widely used in Raman spectroscopy. The analyte dissolved in volatile solvents disperses uniformly and leave a homogeneous distribution of analyte molecules across the substrate with a so-called coffee-ring pattern, i.e. stains of agglomeration of analytes in particular at the boundary of the drying spot [15]. As shown in Figure 1(a), by deliberate design of the EUV-IL mask, it was ensured that after lift-off, four equivalent bare areas are formed on each side of the NP array. Using a micropipette dispenser, a 1 μl drop of 0.1 mg/ml TNT solution was brought onto the substrates. The solution spread to a diameter of ~ 5 mm covering an area much larger than the region where Raman measurements were made and hence an equivalent distribution of analyte both on the bare and the nanostructured areas can be assumed. In Figure 1(b) and (c), false color images of the drop-coated substrate are presented. The TNT deposited on bare area appears highly inhomogeneous. However, the inhomogeneity is not apparent on the nanostructured area. In order to explore this interesting phenomenon, we performed further characterization using atomic force microscopy (AFM). AFM measurements were carried out before and after drop coating 1μL of 0.1 mg/ml TNT on the substrate. In Figures 1(d) and (e), AFM images of coated bare and NP areas, respectively, are presented. While it is clear from the panels on the left that micro-crystals (with a height of about 500 nm, see Supporting Information) are formed on the drop-coated bare areas, this is not observed on nanostructured region. Thus, it could be concluded that the TNT spreads uniformly on the NP arrays while agglomerations are formed on the bare areas, probably due to different surface tension.

Analyst Accepted Manuscript

Figure 2(a) displays RR and DUV-SERRS spectra of TNT deposited on bare areas and NP arrays. The incident optical power was 1 mW and the signals were acquired for 1 s by moving the sample in steps of 25 μm per individual exposure using a piezo-controlled sample stage. 25 spectra were acquired each on NP array as well as bare areas. All the acquired spectra are plotted in light grey. The highlighted spectra in red and black represent the mean of all the 25 measurements each on the NP array and bare areas, respectively. A clear enhancement of the Raman signal from TNT deposited on the NP array is observed. Moreover, it was observed that the variation of the peaks in an individual spectrum is about ±20% from the mean value. This is a very good reproducibility where the variations in the spectra include all the possible effects such as homogeneity of the molecules, uniformity of the NP arrays and defocusing of the microscope over the large areas.

The SNR ratio can be further improved by collecting the Raman signal from more molecules circumventing photodegradation, as discussed later. Figure 2(b) shows the spectra that are obtained by continuously scanning the sample across the incident laser beam during the signal acquisition. This method results in better resolved Raman bands, and significantly improves the SNR. The acquisition time was 2 s and the incident power was kept constant at 1 mW. The sample stage was moved manually by ~ 35 μm during each acquisition. Once again all the acquired spectra are presented in grey and the mean of all the 12 measurements on the NP array (red line) and bare area (black line) are highlighted. A clear increase in the Raman signal from TNT deposited on the NP array is observed. Relative signal enhancement of about an order of magnitude was observed as compared to that on bare substrates. Clearly, the SNR of the spectra acquired by continuously moving the sample stage is much higher than that of 1 s acquisitions at discrete spots. The prominent Raman bands are marked. The most intense ones occur at 1354 cm^{-1} and 1624 cm^{-1}. These bands are generally assigned to NO_2 symmetric stretching and 2,6-NO_2 asymmetric stretching coupled to the aromatic ring stretching, respectively [17, 22]. Apart from these we also observe a small peak at 1555 cm-1. This band is sometimes assigned to O_2 stretching [22] or to the asymmetric nitro stretching [17]. Fewer bands are observed in comparison to liquid state measurements [23] as the molecules are localized on a solid substrate, which reduces the degrees of freedom available to vibrational modes.

Analyst Accepted Manuscript

Raman measurements by sample scanning were performed four times - at two different positions on two NP arrays having similar parameters. The mean of all these measurements are plotted in Figure 3(a). The spectra are displaced vertically for clarity. A and B indicate two different NP arrays both having a periodicity of 200 nm, NP diameter of 80 nm and NP height of 70 nm. In Figure 3(b), the intensity of the Raman band at 1354 cm^{-1} has been plotted from the measurements on both bare as well as NP substrates. The Raman intensity is reproducible and comparable for the two DUV-SERRS substrates.

Given the fact that the spot size of the incident laser beam on the sample is 1 μm and that the deposited 1 μl TNT solution spreads to a 5 mm spot, the ratio of laser spot size to TNT spot size is 4×10^{-8}. Assuming a uniform deposition of TNT over the whole spot, for 0.1 mg/ml solution, we arrive at the mass of the molecules present in the focus to be 4 femtograms, which corresponds to approximately 10 million TNT molecules. It should be noted that this is a highly overestimated value, as it is known that on drop coating, most of the solvent molecules are present on the outer boundary of the formed 'coffee-ring' pattern and crystallites that are formed on bare areas should further reduce the concentration of drying liquid on nanostructured areas. This rough estimation is in accordance with measurements of absorption spectra of drop-coated TNT solution from which we estimate the amount of TNT in a spot of 1 μm diameter about 1 femtograms (see the Supporting Information). Taking the fact into account that we have a high SNR of about 120 and the detection limit can be defined as a SNR of three, the Raman detection limit in this case is about 100 attograms. This is a substantial improvement compared to other detection methods and, in particular, to SERS in the visible and in the NIR range, where the detection limits are on the order of picograms. Thus, the improved sensitivity in combination with the signal reproducibility makes DUV-SERRS based on well-defined Al NP arrays an extremely valuable technique for tracing TNT.

One drawback of UV and DUV Raman scattering is the analyte photodamage caused by the incident high-energy photons, which is further increased under resonant excitation. The higher background noise and broader Raman band close to 1624 cm^{-1} seen in Figure 2(a) could be due to formation of some photodegradation byproducts. As explained in the Supporting Information, the Raman band at this wavenumber decayed more slowly as compared to the one at 1354 cm^{-1}. Moreover, on close observation it can be seen from Figure 1(c) that a dark (less transparent)

Analyst Accepted Manuscript

patch remained at each spot on the NP array where the Raman signal was acquired. Similarly, a trace (see Supporting Information) was left on the sample when the laser beam was scanned for the Raman measurements reported in Figure 2(b). We note that our setup, which uses a CW laser and single stage spectrometer with a Raman edge filter, is very effective against photodegradation. Most of the UV Raman experiments have been performed with pulsed lasers and triple-stage spectrometers and therefore continuous replacement of the analytes is needed in order to obtain reasonable signals.

The surface enhancement observed in this work can be attributed purely to the EM enhancement. The chemical enhancement is not possible since the analyte molecules are not chemisorbed on metallic Al due to the naturally formed oxide layer with a thickness of 3-5 nm. We note that the lack of chemical enhancement [12] can be seen rather as an advantage, since the observed Raman spectra are identical to the spectra of the solid phase analytes, whereas in most cases the interaction of molecules with a metal surface modifies the Raman peaks position and intensities along with the chemical enhancement.

The EM enhancement is achieved when the excitation frequency matches a LSPR. Al NP arrays support strong dipolar and quadrupolar LSPRs in the UV and DUV wavelength region [33]. The position of the LSPR peaks could be easily tuned by varying the NP parameters like the diameter, periodicity and height. This makes Al NP arrays ideal substrates for DUV-SERRS. Large-area NP arrays fabricated using EUV-IL were used to achieve reproducible SERS signal. The NPs are produced in a square lattices over an area of 400 μm × 400 μm, with a periodicity of 200 nm, NP diameter of 80 nm and height of 70 nm. In Figure 4(a) and (b), large-area and high-magnification SEM images, respectively, of Al NP arrays are presented. The extinction spectra of the NP array with and without TNT are plotted in Figure 4(c) (for the details of the measurement method, see the Supporting Information). The strong dipolar resonance mode at 330 nm is red-shifted by ~14 nm after TNT deposition. There is also a small contribution of the quadrupolar resonance mode at the Raman excitation wavelength of 257 nm. Recently, it has been shown that the EM enhancement associated with this mode gives rise to SERS [27].

Simulations based on the finite-difference time-domain (FDTD) method were performed to understand the far-field and near-field optical properties of the NP arrays (for the details, see the Supporting Information). The calculated extinction spectra for arrays of NPs with diameter of 60

Analyst Accepted Manuscript

nm, 80 nm and 130 nm are reported in Figure 5(a). It is observed that the one for 80 nm NPs matches well with the experimental extinction spectrum of the NP arrays used as SERRS substrate. It is also clear that arrays with 130 nm NPs exhibit a stronger quadrupolar resonance mode close to 257 nm, the Raman excitation wavelength, which leads to higher enhancement factors. This is confirmed by near-field calculations performed at this wavelength. Figure 6(a) and (b) display a top-view of the electric field intensity enhancement $|E|^2$ evaluated at the top surface – just outside the oxide shell – for both 130 nm and 80 nm NPs. In Figures 6(c) and (d) the field intensities at the bottom surface of the NPs are presented. The near fields were evaluated at the excitation wavelength. It is found that the intensity enhancement close to the top NP surface and its spatial extent are much higher for 130 nm NPs as compared to those with a diameter of 80 nm. Indeed, the maximum value of $|E|^2$ is ~75 for the former and ~25 for the latter. This is a direct consequence of the more pronounced quadrupolar resonance mode for the larger NP at the excitation wavelength. Since the SERS intensity scales approximately as the fourth power of the electric field, Figure 7 displays the enhancement of $|E|^4$ averaged over an area equivalent to the top NP surface, as a function of distance from it. As expected the field drops off rapidly away from the NP. Therefore, in order to achieve high enhancement factors the analytes deposited on the surface should be sufficiently thin and should not be forming nanocrystallites.

In summary, we have demonstrated a highly sensitive and real-time detection of TNT using large-area Al NP arrays as SERRS substrates in the DUV range. We have shown that a reproducible detection limit of attograms of TNT is within reach. The DUV-SERRS technique outperforms the sensing capabilities of most reported Raman, SERS studies as well as of other well established methods. Hence, it is a highly promising tool for specific detection of explosive materials. We note that the sensitivity can be further improved substantially by appropriate optimization of the geometrical parameters of the Al NPs, such as period, diameter and height. In addition the EM enhancement factors can be increased further by using other types of nanostructures such as nanovoids, nanoholes, triangular NPs, and closely-spaced NP dimers [12, 26, 28, 34, 36]. Therefore, there is a significant potential of improvement in the detection limit of TNT with DUV-SERRS using Al nanostructures that are optimally designed for this purpose. Additionally, the sensitivity can be improved further by optimizing the Raman signal collection and detection systems such as the use of high NA objective, better optics and improved efficiency of the detector.

Analyst Accepted Manuscript

Further studies should include the optimization of Al nanostructures, the detection system, and extending the analysis to other explosive materials. A systematic study of immobilizing the analytes on the SERS substrates should be undertaken. This includes appropriate collecting, preconcentrating, and drop-coating methods to bring the molecules in contact with the Al nanostructures. Moreover, since NP arrays exhibit modified wetting properties, Al nanostructured surfaces may also be exploited to selectively increase the analyte concentration by elaborative control of the surface tension [37]. Lastly, with increasing availability of low cost, compact DUV lasers, a SERRS based portable explosive detection system can be feasible and can offer unmatched sensitivity with high specificity.

Supporting Information Available

More details on sample preparation, TNT absorption, SERRS intensity decay measurements, trace of photodegradation byproduct, AFM measurements and FDTD simulations. This material is available free of charge via the Internet at http://pubs.acs.org.

Acknowledgement

The authors would like to thank Michaela Vockenhuber and M. K. Singh for their technical assistance. Part of this work was performed at the Swiss Light Source (SLS), Paul Scherrer Institute, Switzerland.

References

1. Marshall, M.; Oxley, J. C., Eds.; *Aspects of explosives detection,* Elsevier, Amsterdam, 2009.

2. Steinfeld, J. I.; Wormhoudt, J. *Annu. Rev. Phys. Chem.* **1998**, 49, 203-232.

3. Moore, D. S. *Rev. Sci. Instrum.* **2004**, 75, 2499-2512.

4. Steevens, J.A.; Duke, B. M.; Lotufo, G. R.; Bridges, T. S. *Environ. Toxicol. Chem.* **2002**, 21, 1475-1482.

5. Robidoux, P.Y.; Bardai, G.; Paquet, L.; Ampleman, G.; Thiboutot, S.; Hawari, J.; Sunahara, G.I. *Arch. Enviro. Contam.Toxicol.* **2003**, 44, 198-2009.

6. Kartha, K. K.; Babu, S. S.; Srinivasan, S.; Ajayaghosh, A. *J. Am. Chem. Soc.*, **2012**, 134, 4834-4841.

Analyst Accepted Manuscript

7. Moore, D.S.; Scharff, R. J. *Anal. Bioanal. Chem.* **2009**, 393, 1571-1578.

8. Ehlerding, A.; Johansson, I.; Wallin, S.; Östmark, H. *Proc. SPIE* **2010**, 7835, 783507-1 - 783507-7.

9. Gaft, M.; Nagli, L. *Opt. Mater.* **2008**, 30, 1739-1746.

10. Moskovits, M. *Rev. Mod. Phys.* **1985**, 57, 783–826.

11. Stiles, P. L.; Dieringer, J. A.; Shah, N. C.; Van Duyne, R. P. *Annu. Rev. Phys. Chem.* 2008, 1, 601-6026.

12. Le Ru, E. C.; Etchegoin, P. G. *Principles of Surface-Enhanced Raman Spectroscopy*; Elsevier, Amsterdam, 2009.

13. Kneipp, K.; Wang, Y.; Dasari, R. R.; Feld, M. S.; Gilbert, B. D.; Janni, J.; Steinfeld, J. I. *Spectrochim. Acta Mol. Biomol. Spectros.* **1995**, 51, 2171-2175.

14. Tao, A.; Kim, F.; Hess, C.; Goldberger, J.; He, R.; Sun, Y.; Xi, Y.; Yang, P. *Nano Lett.* **2003,** 3, 1229-1233.

15. Botti, S.; Cantarini, L.; Palucci, A. *J. Raman Spectrosc.* **2010**, 41, 866-869.

16. Liu, X.; Zhao, L.; Shen, H.; Xu, H.; Lu, L. *Talanta* **2011**, 83, 1023-1029.

17. Jerez-Rozo, J. I.; Primera-Pedrozo, O. M.; Barreto-Caban, M. A.; Hernandez-Rivera, S. M. *IEEE Sensors Journal* **2008**, 8, 974-982.

18. Liu, H.; Lin, D.; Sun, Y.; Yang, L.; Liu, J. *Chem. Eur. J.* **2013,** 19, 8789-8796.

19. Yang, L.; Ma, L.; Chen, G.; Liu, J.; Tian, Z.-Q. *Chem. Eur. J.* **2010**, 16, 12683-12693.

20. Zhou, X.; Liu, H.; Yang, L.; Liu, J. *Analyst* **2013**, 138, 1858-1864.

21. Asher, S. A.; Johnson, C. R. *Science* **1984**, 225, 311-313.

22. Tuschel, D. D.; Mikhonin, A. V.; Lemoff, B.E.; Asher, S. A. *Appl. Spectrosc.* **2010**, 64, 425-432.

23. Ghosh, M.; Wang, L.; Asher, S. A. *Appl. Spectrosc.* **2012**, 66, 1013-1021.

24. Nagli, L.; Gaft, M.; Fleger, Y.; Rosenbluh, M. *Opt. Mater.* **2008**, 30, 1747-1754.

25. Ehlerding, A.; Johansson, I.; Wallin, S.; Östmark, H. *Int. J. Spectrosc.* **Volume 2012**, Article ID 158715.

Analyst Accepted Manuscript

26. Yang, Z. -L.; Li, Q. -H.; Ren, B.; Tian, Z. -Q. *Chem. Commun.* **2011**, 47, 3909-3911.

27. S. K. Jha, Z. Ahmed, M. Agio, Y. Ekinci, and J. F. Löffler, *J. Am. Chem. Soc.* **2012**, 134, 1966-1969.

28. Sigle, D. O.; Perkins, E.; Baumberg, J. J.; Mahajan, S. *J. Phys. Chem. Lett.* **2013**, 4, 1449−1452.

29. Ekinci, Y.; Solak, H. H.; Löffler, J. F. *J. App. Phys.* **2008**, 104, 083107-1 - 083107-6.

30. Langhammer, C.; Schwind, M.; Kasemo, B.; Zoric, I. *Nano Lett.* **2008**, 8, 1461.

31. Chen, G. H.; Zhao, J.; Schatz, G. C.; Van Duyne, R. P. *J. Phys. Chem. C* **2008** 112, 13958-13963.

32. Chowdhury, M. H.; Ray, K; Gray, S. K.; Pond. J; Lakowicz, J. R. *Anal Chem.* **2009**, 81, 1397–1403.

33. Knight, M.; Liu, L.; Wang, Y.; Brown, L.; Mukherjee, S.; King, N. S.; Everitt, H. O.; Nordlander, P.; Halas, N. J. *Nano Lett.* **2012**, 12, 6000–6004.

34. McMahon, J. M.; Schatz, G. C.; Gray, S, K. *Phys. Chem. Chem. Phys.* **2013**, 15, 5415-5423.

35. Päivänranta, B.; Langner, A.; Kirk, E.; David, C.; Ekinci, Y. *Nanotechnology* **2011**, 22, 375302.

36. Cheng, Y.; Wang, M.; Borghs, G.; Chen H. *Langmuir,* **2011**, 27, 7884-7891.

37. De Angelis, F.; Gentile, F.; Mecarini, F.; Das, G.; Moretti, M.; Candeloro, P.; Coluccio, M. L.; Cojoc, G.; Accardo, A.; Liberale, C.; Zaccaria, R. P.; Perozziello, G.; Tirinato, L.; Toma, A.; Cuda, G.; Cingolani, R.; Di Fabrizio, E. *Nature Photon.* **2011**,5, 682–687.

Analyst Accepted Manuscript

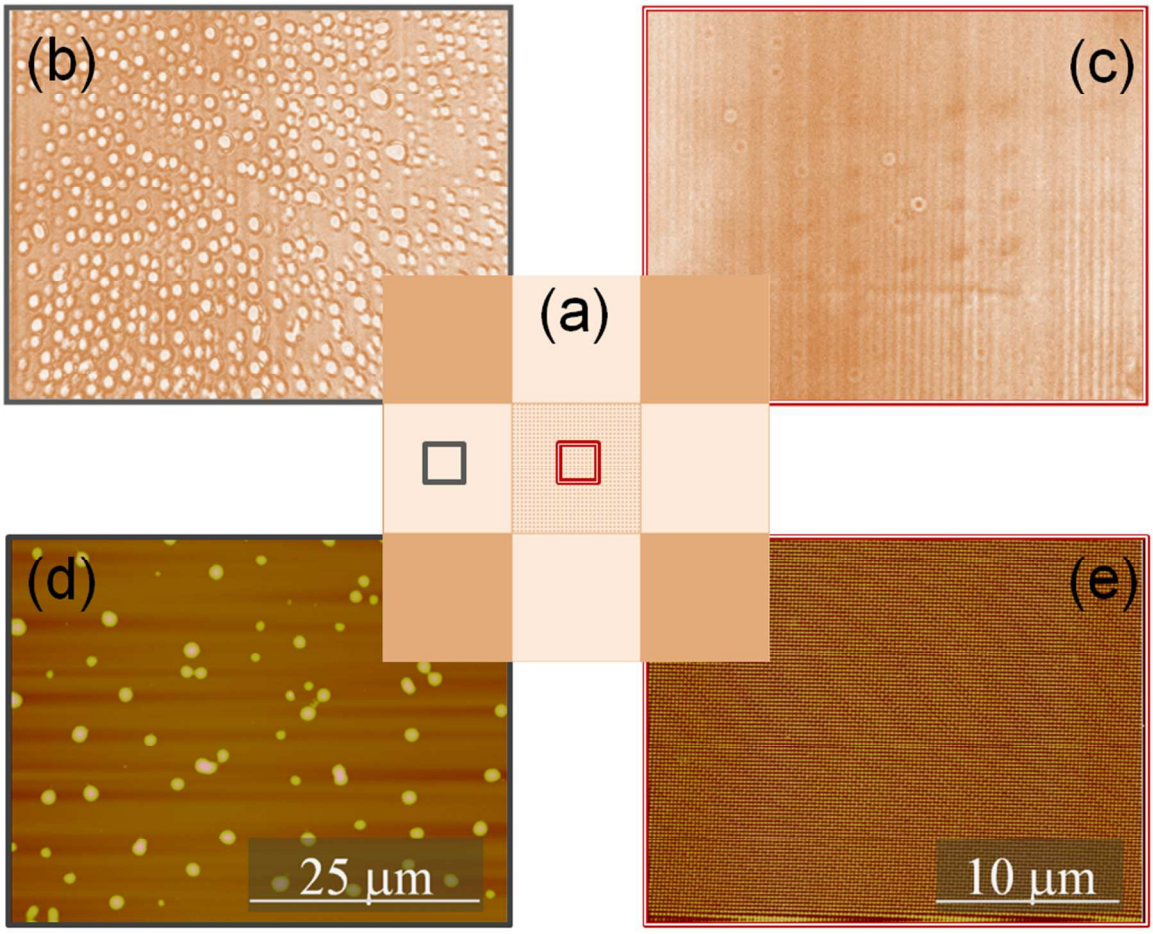

Figure 1. (a) Schematic representation of the substrate that results after the EUV-IL with Al NP array in the center surrounded by four equivalent bare areas. The size of the central region is 400 µm × 400 µm. Optical image of the bare area (b), NP array (c) after drop-coating the sample with 0.1 mg/ml TNT solution. AFM images of TNT coated bare substrate (d) and NP array(e). All the panels are outlined with appropriate colors to indicate the region on the sample where the images were acquired.

Analyst Accepted Manuscript

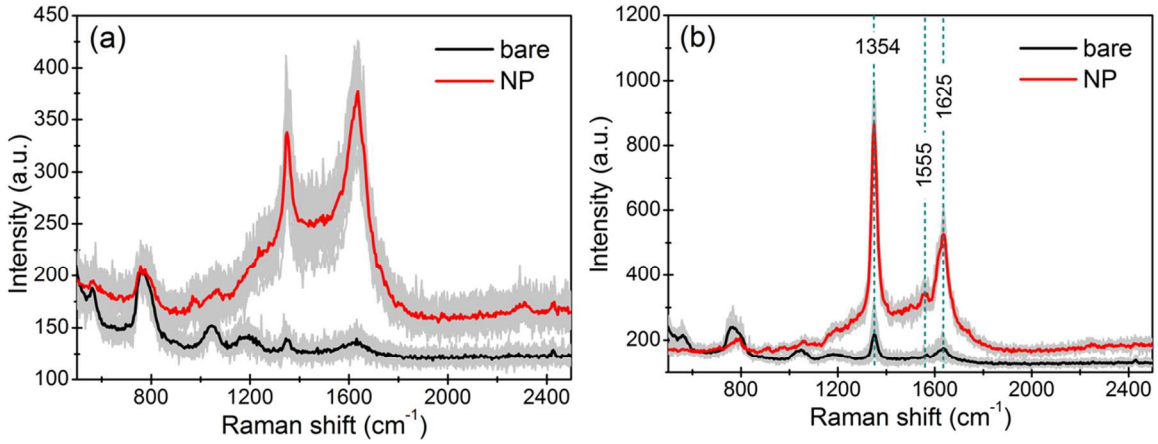

Figure 2: (a) Raman spectra of 0.1 mg/ml TNT deposited on bare and NP array areas. Exposure time was 1 s and incident optical power was 1 mW. 25 spectra were acquired both on the NP arrays and bare areas in a 5 × 5 matrix while moving the sample stage in steps of 25 μm after each measurement. The highlighted spectra represent the mean of all the spectra acquired over the NP array (red line) and bare areas (black line). (b) RR and SERRS acquired while continuously moving the sample stage during signal acquisition. Exposure time was 2 s and incident optical power was 1 mW. The highlighted spectra represent the mean of multiple spectra acquired over the NP array (red line) and bare areas (black line).

Analyst Accepted Manuscript

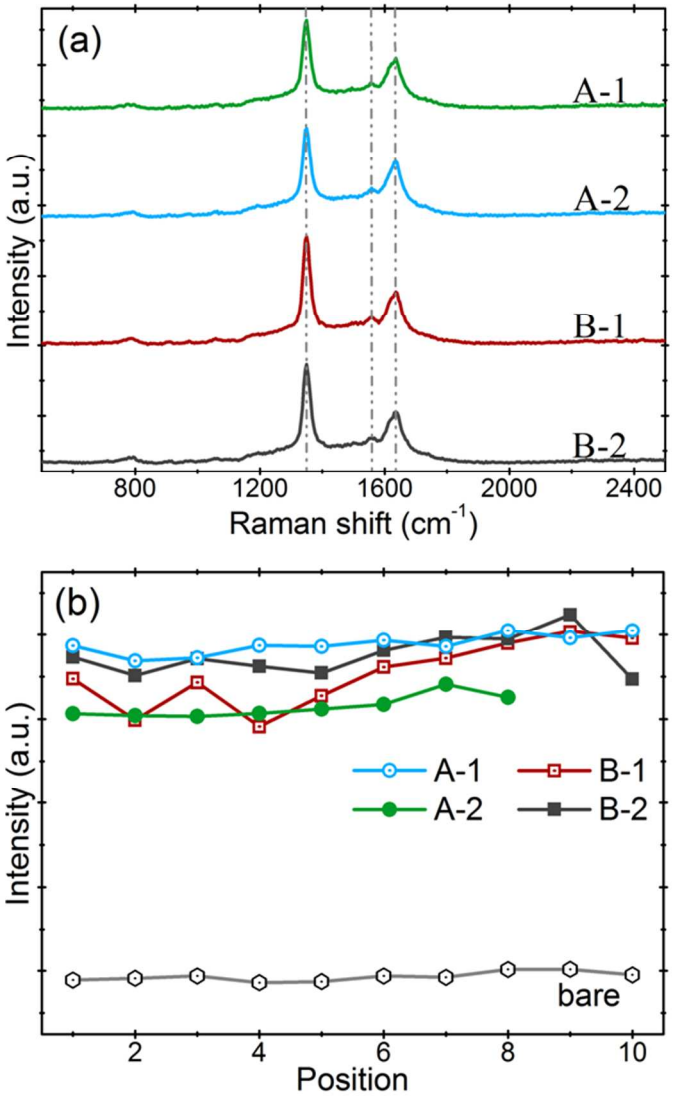

Figure 3: (a) Raman spectra of TNT acquired at different locations (1 and 2) on NP arrays A and B having similar NP parameters: period = 200nm, NP height = 70 nm and NP diameter = 80 nm. (b) Reproducibility of peak intensities of the 1354 cm^{-1} Raman band of TNT measured at different positions on fused silica and NP arrays.

Analyst Accepted Manuscript

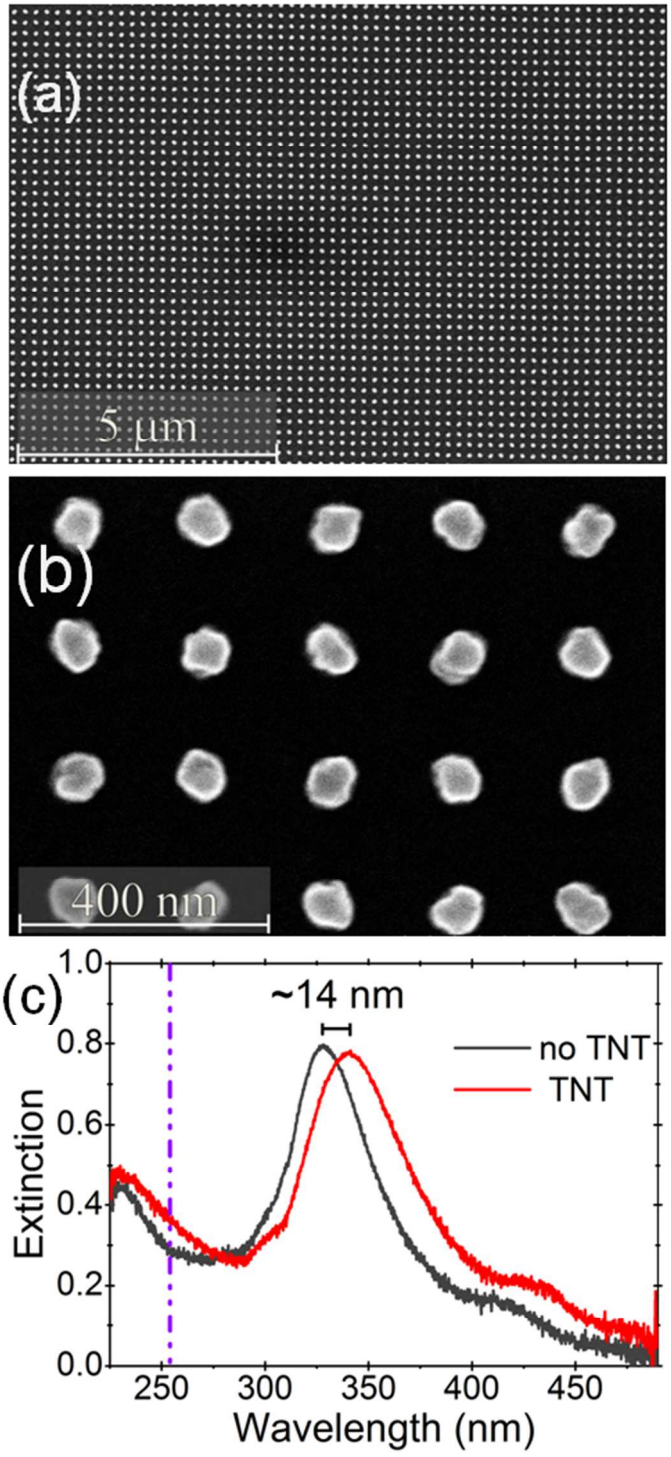

Figure 4: Large-area (a) and high-magnification (b) SEM images of the Al NP array. (c) Extinction spectra of the NP array with and without deposited TNT.

Analyst Accepted Manuscript

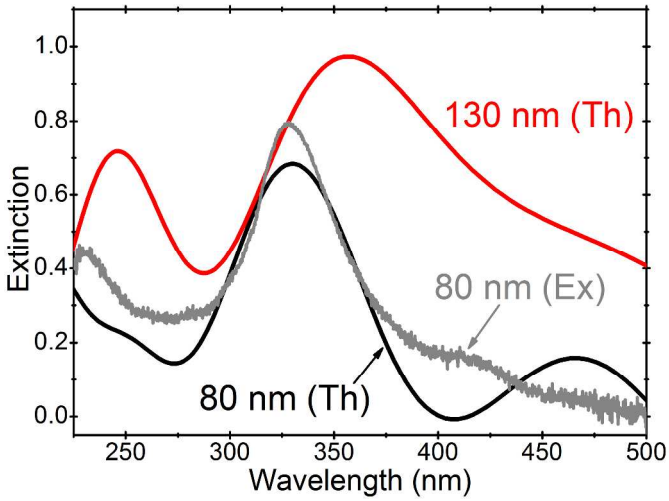

Figure 5: Calculated (Th) extinction spectra of Al NP arrays, with diameters 80 nm and 130 nm, period 200 nm and NP height 70 nm, are compared to experimental (Ex) extinction spectrum of NP array having a NP diameter of 80 nm.

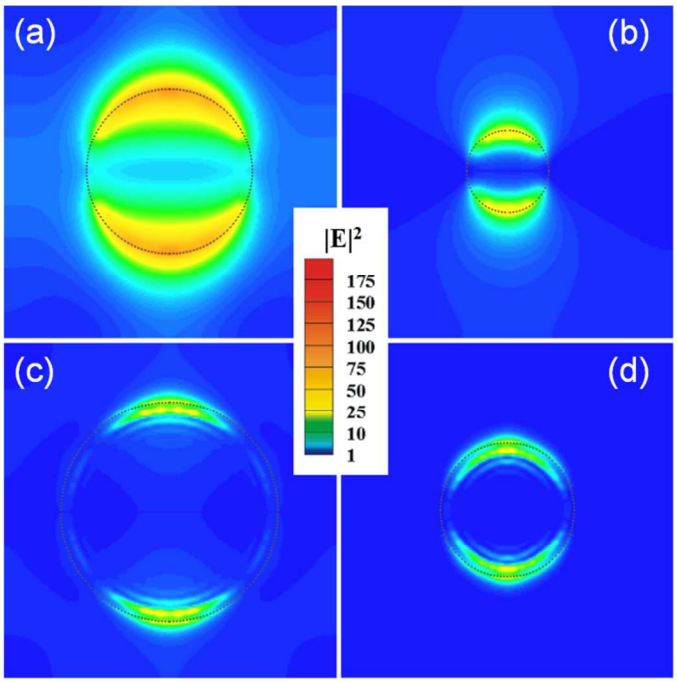

Figure 6: Calculated electric field intensity enhancement $|E|^2$ for Al NP arrays having a NP diameter of 130 nm ((a) and (c)) and 80 nm ((b) and (d)). In (a) and (b) the field intensity on top-surface, just above the oxide-shell is presented. In (c) and (d) the field intensity at the bottom NP surface is shown. The NP extent is marked by the overlaid circle.

Analyst Accepted Manuscript

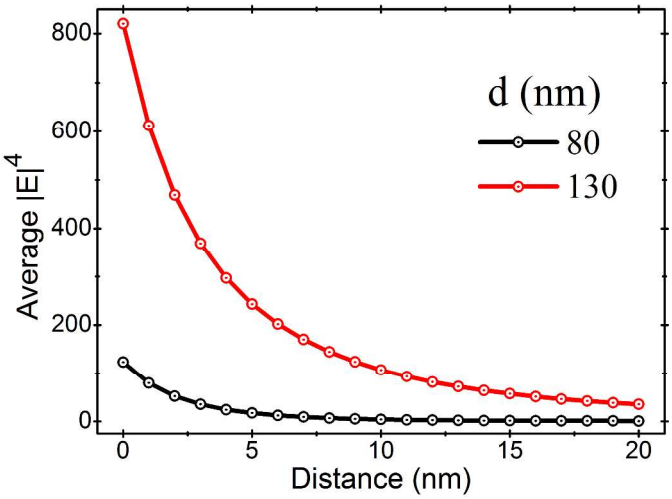

Figure 7: Average $|E|^4$ enhancement calculated at various distances above the NP top surface (outside the oxide shell) for 80 nm and 130 nm NP diameters.

Analyst Accepted Manuscript